Nano Research Energy

ISSN 2791-0091 (print); 2790-8119 (online)
https://doi.org/10.26599/NRE.2024.9120133

Research Article

Electron/ion-conductive and flexible dual-functional copolymer enabled by EDOT and h_2PDMS for optimized Li-ion batteries

Jingwei Wang[1], Zhaowen Bai[2], Zejia Zhao[3], Guangping Zheng[4], Junye Cheng[1] (✉), and Guohua Chen[2] (✉)

[1] *Department of Materials Science, Shenzhen MSU-BIT University, Shenzhen 517182, China*
[2] *School of Energy and Environment, City University of Hong Kong, Tat Chee Avenue, Kowloon, Hong Kong, China*
[3] *Institute of Semiconductor Manufacturing Research, College of Mechatronics and Control Engineering, Shenzhen University, Shenzhen 518060, China*
[4] *Department of Mechanical Engineering, The Hong Kong Polytechnic University, Hung Hom, Kowloon, Hong Kong, China*

Received: 9 May 2024 / **Revised:** 2 July 2024 / **Accepted:** 4 July 2024

ABSTRACT

Electron/ion-conductive flexible copolymer PEDOT-PDMS (poly(3,4-ethylenedioxythiophene)-poly(dimethylsiloxane)) was successfully developed, which not only effectively optimizes high-voltage $NaLiFePO_4F$ cathode through dripping on electrode surface but also improves high-capacity Si anode through *in-situ* polymerization on the surface of Si particles. Theoretical calculation and experiments indicate that π-π conjugated structure in PEDOT-PDMS molecular chains easily interacts with PF_6^- anions, providing electron transfer pathways and preventing HF production. Moreover, Li ions transfer through Si-O in the amorphous phase of the copolymer, and its Young's modulus at rupture is 1.17±0.10 MPa. The *in-situ* TEM results directly confirm that the polymer layer provides conducting pathways and buffers the stress induced by lithiation. With the $NaLiFePO_4F$ coated cathode, the cells show good cycle stability (~100% of capacity retention after 500 cycles) and high chemical diffusion coefficient of lithium-ions (1.89×10^{-9} $cm^2\cdot s^{-1}$ and 1.20×10^{-9} $cm^2\cdot s^{-1}$). In the case of coated Si anode, a capacity of 1512 $mAh\cdot g^{-1}$ is retained after 1000 cycles at 0.5 C with a capacity retention of 69.8% in terms of the highest specific capacity around the 160th cycle. This work opens a new avenue for the simultaneous optimization of cathode and anode with a functional polymer.

KEYWORDS

PEDOT-PDMS, electron and ionic conductive, flexible, $NaLiFePO_4F$ cathode, Si anode

1 Introduction

Li-ion batteries have been one of the most attractive novel energy storage systems for powering electric devices because of their intrinsic advantages such as high energy density, high efficiency, and no memory effect [1–3]. With increasing energy demand for electric vehicles (500 km drive range after one charging event), the costs of Li-ion battery packs, and their safety have to be further optimized [4, 5].

Low-cost $NaLiFePO_4F$ is a promising candidate because of its framework connectivity which could show high potential. It is attributed to the inductive effect of PO_4^{3-} group and electron-withdrawing characteristic of F^-. In addition, the Na^+ ions with relatively larger size could enhance the structural stability. Unfortunately, $NaLiFePO_4F$ is significantly sensitive to hydrofluoric (HF) acid generated during the operation of batteries ($LiPF_6 \rightleftharpoons LiF + PF_5$, $PF_5 + H_2O \rightarrow POF_3 + 2HF$). Furthermore, its electronic conductivity should also be improved. As for anode, Si has been considered to be one of the most promising materials for next-generation lithium-ion batteries due to the well known high theoretical capacity (4200 $mAh\cdot g^{-1}$, based on the full lithiation reaction with the formation of $Li_{22}Si_4$), about ten times that of commercial graphite anode, low lithiation voltage plateau (0.2–0.3 V vs. Li/Li^+) that could avoid the undesirable lithium plating and formation of lithium dendrite and consequently improve safety, abundance on the earth (the second abundant element, 28% by mass), good environmental compatibility, low toxicity, and good chemical stability, which is comparable to lithium metal [6–8]. Unfortunately, several drawbacks limit its wide industrial applications, such as significant volume expansion (~300%–400%), low electronic conductivity (10^{-3} $S\cdot cm^{-1}$,) and lithium diffusion capability (10^{-14} and 10^{-13} $cm^2\cdot s^{-1}$) [9]. The specific energy density equation:

$$E = \int_0^Q V(q)\mathrm{d}q/wt \quad (1)$$

shows that the specific capacity $C = \int_0^Q \mathrm{d}q/wt$ and working voltage are directly related to energy density.

Therefore, it is vital to optimize the efficiency of $NaLiFePO_4F$ cathode and Si anode. Taking into account the attempts of surface

Address correspondence to Junye Cheng, chengjunye@smbu.edu.cn; Guohua Chen, ghchen1963@gmail.com

modifications made to adjust the physical and chemical performances of electrode materials, surface coating at the level of active material or prepared electrode is a facile approach to improve electrical conductivity and provide surface protection [10, 11]. However, the conventional coating materials are brittle and weak in adhesion, which could lead to delamination from the surface and thus diminish its performance [12]. In addition, these coating materials are of low ions and/or electrons conductivity, decreasing the rate performance and increasing the irreversible capacity of the batteries.

Conducting polymers have been broadly applied in the modifications of electrode materials in batteries. Recently, polymers, especially, three of the most well-known conducting polymers, poly (3,4-ethylenedioxythiophene) (PEDOT), polypyrrole (PPy) and polyaniline (PANI), have been considered as promising type of surface coating materials [13, 14]. They are electrochemically and thermally stable in batteries. In our original group, Chen et al. reported an oCVD technique to build a protective conductive PEDOT skin on cathode materials [15], and Cheng et al. reviewed the protective coating used for Li metal [16]. The capability of these three polymers decreases in the order of PEDOT > PPY > PANI [17]. Nevertheless, they do not occupy the capability of conducting Li^+ ions and present relatively poor flexibility. Hence, it is important to develop a polymer with high electrical and ionic conductivity, as well as good flexibility, and at the same time, it can absorb HF or prevent HF generation, implementing the optimization on both $NaLiFePO_4F$ cathode and Si anode. Among the aforementioned polymers, poly(dimethylsiloxane) (PDMS) has also attracted much attention. It has been used as a stable interfacial layer for high-performance Li-metal batteries due to its mechanical flexibility and chemical stability [18, 19].

Herein, the desired copolymer PEDOT-PDMS can be successfully synthesized based on h_2PDMS and EDOT monomer, optimizing efficiency of $NaLiFePO_4F$ cathode and Si anode. The reaction occurs between ethylenedioxythiophene (EDOT) conductive skeleton and flexible hydride terminated poly(dimethylsiloxane) (h_2PDMS) with the assitant of Karstedt catalyst. The PF_6^- anions easily interact with the conjugate structure in PEDOT-PDMS, leading to less amount of PF_5 in the electrode and subsequently less HF. In addition, π-π conjugated structure provides electron transfer pathways and Li^+ ions transfer through Si-O in the amorphous phase. The *in-situ* TEM results directly confirm that the polymer coating layer provides conducting pathways and buffers the stress. Young's modulus of copolymer film at rupture is 1.17±0.10 MPa. Remarkably, $NaLiFePO_4F$ coated cathode shows good cycle stability (~100% of capacity retention after 500 cycles) and Si anode endows a capacity of 1512 mAh·g^{-1}, which is retained after 1000 cycles at 0.5C with a capacity retention of 69.8% in terms of the highest specific capacity.

2 Experimental

Details of the experimental section are provided in the Electronic Supplementary Material (ESM).

3 Results and discussion

PEDOT-PDMS polymer is synthesized through the hydrosilylation and dehydrocoupling reaction that occurred between h_2PDMS and the EDOT monomer (Fig. 1(a)). The hydrosilylation reaction occurs between Si-H and C=C groups, and dehydrocoupling reaction occurs simultaneously between Si-H (C-H) and C-H in the presence of Karstedt catalyst, as shown in Fig. 1(b). The solution before the reaction is nearly transparent (Fig. S1 in the ESM). However, it changes to yellowish after the reaction with Karstedt catalyst, indicating that the reaction has taken place.

To identify the product resulting from the reaction between EDOT and h_2PDMS, the Fourier transform infrared spectroscopy (FTIR) spectra of h_2PDMS and PEDOT-PDMS are measured, as shown in Fig. 1(c). The peaks around 2958 and 2900 cm^{-1} are attributed to stretching vibrations of CH_3 groups; the peaks at 1411 and 1260 cm^{-1} are assigned to the deformation vibration and symmetrical vibrations of CH_3 groups; the peak at 793 cm^{-1} is due to the CH_3 rocking vibration and the Si-C stretching vibration; the peaks at 1085 and 1030 cm^{-1} are assigned to the asymmetric and symmetric stretching of Si-O-Si for PDMS, respectively [20]. Obviously, the characteristic Si-H group at 2131 and 908 cm^{-1} has disappeared, providing evidence that there occurs the reaction

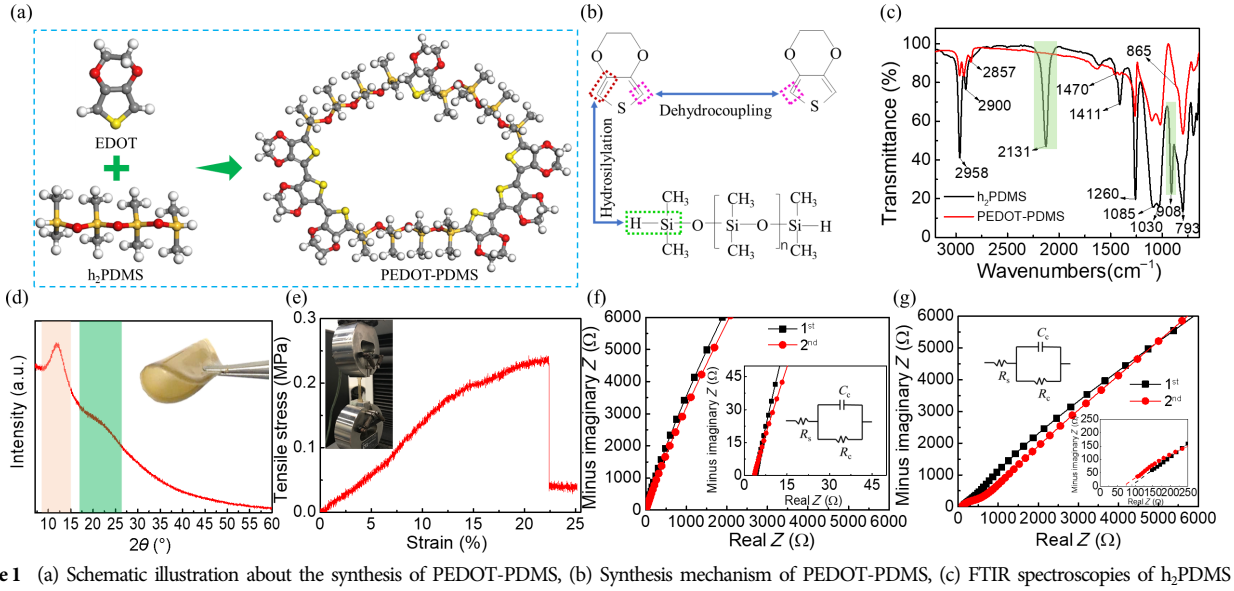

Figure 1 (a) Schematic illustration about the synthesis of PEDOT-PDMS, (b) Synthesis mechanism of PEDOT-PDMS, (c) FTIR spectroscopies of h_2PDMS and PEDOT-PDMS, (d) XRD patterns and (e) stress-strain curve of PEDOT-PDMS film (inset shows photo of film). EIS of (f) SS electrode and (g) SS@PEDOT-PDMS electrode in symmetrical cells after the first and the second cycles along with equivalent circuit.

between h_2PDMS and EDOT [21]. Some new peaks can be observed in FTIR spectroscopy of PEDOT-PDMS. The new peaks around 1470 and 2857 cm^{-1} are attributed to the C=C band and symmetric CH_2 stretching, respectively [22]. The characteristic peak around 865 cm^{-1} for the Si-C bond overlaps with those for the CH_3 rocking vibration and the Si-C stretching vibration. The measurement on nuclear magnetic resonance (NMR) spectra of EDOT, h_2PDMS, and PEDOT-PDMS are further conducted (Fig. S2 in the ESM). Signals 1(C=CH) and 2 (CH_2) are assigned to EDOT monomer [23]. Signals 3 (Si-H) and 4 (CH_3) are assigned to h_2PDMS [24]. The characteristic C=CH and Si-H signals are used to evaluate the reaction between EDOT and h_2PDMS. After the reaction, the C=CH signal disappears while the CH_2 signal remains unchanged. In addition, the Si-H signal disappears and the CH_3 signal is also unchanged. A new signal 5 at around 1.55 ppm appears, which can be associated with the CH group. Hence, the PEDOT-PDMS product can be confirmed initially by using FTIR and NMR spectra.

The X-ray diffraction (XRD) patterns of PEDOT-PDMS film shows no sharp peaks except two broad peaks (Fig. 1(d)). The broad peaks located at 2θ=8.5°–14.9° and 17.1°–26.2° are ascribed to the amorphous phase of PEDOT-PDMS [25]. In general, the amorphous phase is more ductile than crystalline phase and can accelerate the transfer of Li^+ ions [26]. The mechanical properties of PEDOT-PDMS are investigated to test its flexibility (Fig. 1(e)). A brown film forms after drying the reacted solution, which can be bent without fracture. The film exhibits elastic and plastic behavior. The tensile stress and strain at rupture are 0.24± 0.03 MPa and 22.4±2.1%, respectively. The Young's modulus (elastic modulus) is 1.17±0.10 MPa. The PEDOT film shows brittle behavior with a Young's modulus of 284 MPa and a strain at rupture of 8.5% [27]. In addition, the Young's modulus of PDMS sheet is 605 kPa [28]. In comparison, the copolymer PEDOT-PDMS film is more flexible than PEDOT film and more brittle than PDMS film, making it more feasible to modify electrode materials. In the PEDOT-PDMS film, molecules can form a helix structure because of the corresponding rotations around the highly flexible Si-O bonds, leading to good mechanical properties [29].

To evaluate the conducting property of the PEDOT-PDMS film, the electrochemical impedance spectroscopy (EIS) curves of symmetrical cells assembled with stainless steel sheets as electrodes (SS//SS) is shown in Fig. 1(f). The EIS curves of symmetrical cells assembled with stainless steel sheet coated by PEDOT-PDMS film as electrodes (SS@PEDOT-PDMS//SS@PEDOT-PDMS) is shown in Fig. 1(g). It should be noted that the first EIS is performed after the cells rest for 2 min and the second cycle is performed after resting for 15 h. The total resistance of bulk (R_b) and charge transfer (R_{ct}) for SS//SS at the first cycle (4.0 Ω) is close to the total resistance at the second cycle (3.6 Ω), which can be obtained from the intersection of the linear portion of the curve and the x-axis. However, for SS@PEDOT-PDMS//SS@PEDOT-PDMS, the total resistance (R_b+R_{ct}) is about 85.9 Ω in the first cycle, which is much higher than that of SS//SS due to the resistance of PEDOT-PDMS layer. However, it decreases to 69.1 Ω after the second cycle. The conductivity can be determined by Eq. (2):

$$\sigma = qp\mu \quad (2)$$

where q is the unit charge (1.6×10^{-19} C), ρ and μ are carrier concentration and mobility, respectively. The carrier concentration is directly related to the doping level. At first, there is no dopant in PEDOT-PDMS, but the dopants (PF_6^- in electrolyte) in PEDOT-PDMS increase with cycles. More anion dopings coupled to π-π conjugated structure can result in electron conduction [30]. Hence, the carrier concentration in PEDOT-PDMS increases with increasing cycling number, leading to an increase in conductivity. In addition, the linear portion of the curve is not parallel to the y-axis, indicating the Li^+ ion transportation. The Si-O segments can lead to an amorphous structure that offers a sufficient Li^+ ion mobile pathway [31]. The results indicate that the copolymer PEDOT-PDMS could provide Li^+ transfer pathway resulting from the amorphous phase and become conductive because of the conjugated structure. Meanwhile, it has good mechanical properties. Therefore, the results demonstrate that PEDOT-PDMS can be used to improve the performance of $NaLiFePO_4F$ electrode and Si anode.

$NaLiFePO_4F$ electrode@PEDOT-PDMS is prepared by applying the PEDOT-PDMS solution on the surface of each electrode made of $NaLiFePO_4F$ as active material (Fig. 2(a)). The PEDOT-PDMS layer and the contact between PEDOT-PDMS and $NaLiFePO_4F$ electrode can be observed from cross-sectional scanning electron microscopy (SEM) image of the coated electrode (Fig. 2(b)). The thickness of the coating is uneven because of the pothole of $NaLiFePO_4F$ electrode. The section marked with the yellow line is $NaLiFePO_4F$ electrode and the red line section is PEDOT-PDMS layer. The good contact and compatibility between $NaLiFePO_4F$ and coating are observed. The surface of the coated electrode is smooth while the surface of the bare electrode is rough (Figs. 2(c) and 2(d)). In EDS spectra of $NaLiFePO_4F$ electrode@PEDOT-PDMS, there are no peaks for the elements of $NaLiFePO_4F$ electrode (Fig. S3 in the ESM). The element S is not present in the coated electrode because its content is lower than the detection limit. This result demonstrates that $NaLiFePO_4F$ electrode has been protected by the PEDOT-PDMS coating. The protected layer does not affact the crystalline structure of $NaLiFePO_4F$ electrode (Fig. 2(e)). In addition, the X-ray photoelectron spectra (XPS) results of PEDOT-PDMS sample and $NaLiFePO_4F$ electrode@PEDOT-PDMS electrode exhibit similar spectra (Fig. 2(f)). The representative peaks of C 1s, O 1s, Si 2s, Si 2p, S 2s and S 2p are detected in the spectra, and no other peaks appear. The peak at 100.4 eV is assigned to the new Si-C bond in PEDOT-PDMS. The XPS results further indicate the formation of the compact PEDOT-PDMS layer on the surface of $NaLiFePO_4F$ electrode.

The PEDOT-PDMS coating can enhance the charge transfer at the interface between electrolyte and electrode, which can be confirmed by the EIS of $NaLiFePO_4F$ electrode with different thickness of PEDOT-PDMS coating (Fig. S4 in the ESM). The charge transfer resistance (R_{ct}) for $NaLiFePO_4F$ control, $NaLiFePO_4F$ coated with coating of 1 and 3 μm are around 180, 163 and 140 Ω, respectively. In contrast, the $NaLiFePO_4F$ with thick coatings (5 and 6 μm in thickness) exhibit larger charge transfer resistance because the charge diffusion path in the coating during the electrochemical reaction is longer. The large charge transfer resistance could lead to polarization including the internal resistance drop and the concentration polarization, and then result in poor charge/discharge efficiency and finally the loss of active material and capacity decay. Hence, the electrode shows a lower initial capacity, a longer capacity increase, and poor cycle stability, obtaining a capacity retention rate of only 82.1% after 200 cycles at a current rate of 0.2 C (Fig. S5 in the ESM). The thick coating could delay electrode activation, so it takes a long time for the cells fabricated with an electrode with the thick coating to reach a stable capacity. The $NaLiFePO_4F$ electrodes coated by thicknesses of 1 and 3 μm exhibit an improvement in specific capacity. The

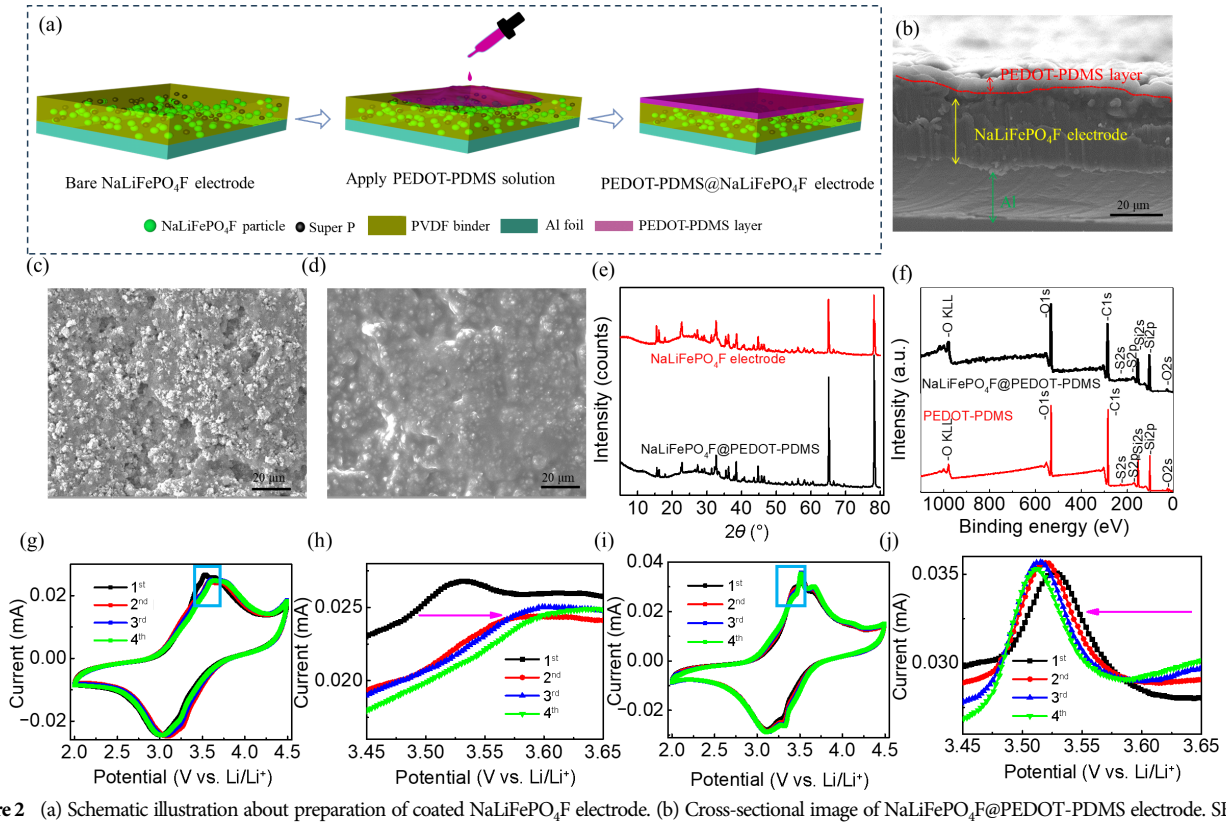

Figure 2 (a) Schematic illustration about preparation of coated $NaLiFePO_4F$ electrode. (b) Cross-sectional image of $NaLiFePO_4F$@PEDOT-PDMS electrode. SEM of (c) $NaLiFePO_4F$ electrode, (d) $NaLiFePO_4F$@PEDOT-PDMS electrode, (e) XRD and (f) XPS of $NaLiFePO_4F$ electrode and $NaLiFePO_4F$@PEDOT-PDMS electrode. CV curves of (g) and (h) $NaLiFePO_4F$ control electrode and (i) and (j) $NaLiFePO_4F$ electrode@PEDOT-PDMS.

discharge capacities of the $NaLiFePO_4F$ control, $NaLiFePO_4F$ with the coating 1 μm in thickness, and $NaLiFePO_4F$ with coating 3 μm in thickness are initially at 94.7, 102.3, and 115.5 $mAh·g^{-1}$, but they change to 91.5, 100.1, and 113.8 $mAh·g^{-1}$ after 200 cycles, corresponding to 96.6%, 97.8%, and 98.5% of the specific capacity retention, respectively. The results indicate that the coating can protect $NaLiFePO_4F$, resulting in no loss of active material and high capacity. Thus, the thickness of the PEDOT-PDMS layer plays an important role in improving the cycle performance of the $NaLiFePO_4F$ electrode. On the other hand, to verify whether PEDOT-PDMS material contributes to the capacity of the whole battery, the batteries with bare PEDOT-PDMS electrode as cathode and Li foil as a reference electrode are examined under the same conditions. The bare PEDOT-PDMS electrode is prepared by applying the PEDOT-PDMS solution on the surface of Al foil directly without binder and super P. The specific capacity of the bare PEDOT-PDMS electrode is very small but very stable even after 200 cycles (Fig. S6 in the ESM), indicating a negligible contribution to capacity and stable chemical and electrochemical properties of PEDOT-PDMS material. The cyclic voltammetry (CV) plot of the bare PEDOT-PDMS electrode further indicates good electrochemical stability (Fig. S7 in the ESM).

The CV plots for the $NaLiFePO_4F$ control and PEDOT-PDMS coated $NaLiFePO_4F$ electrode are obtained in the potential range of 2.0–4.5 V at a scan rate of 0.1 $mV·s^{-1}$. Typically, the anodic peak at the potential of ~3.53 V corresponds to oxidation of Fe from Fe^{2+} to Fe^{3+} [32]. For the $NaLiFePO_4F$ control electrode, the anodic peak at the potential of 3.53 V shifts to a high potential (~3.62 V) after the first cycle, which is related to the kinetic limitations of the control electrode (Figs. 2(g) and 2(h)). While for PEDOT-PDMS coated $NaLiFePO_4F$ electrode, the anodic peak gradually shifts to a lower potential with cycling (Figs. 2(i) and 2(j)), indicating that the introduction of PEDOT-PDMS can lead to a decrease in polarization effect and an improvement in electrochemical performance. Furthermore, it can be indicated from the CV curves that the redox peak currents of PEDOT-PDMS coated $NaLiFePO_4F$ electrode are higher than that of the $NaLiFePO_4F$ control electrode, indicating higher Li insertion capacity. As a result, PEDOT-PDMS on the surface of the prepared $NaLiFePO_4F$ electrode is supposed to effectively facilitate the ions and electrons transport and finally enhance the reaction kinetics for the effective use of $NaLiFePO_4F$ active material, which will further be confirmed by using Galvanostatic intermittent titration technique (GITT) measurement.

The GITT is a reliable method to evaluate the chemical diffusion coefficient of lithium-ions (D_{Li^+}) during cycling. It was employed to determine the D_{Li^+} of $NaLiFePO_4F$ control electrode and the PEDOT-PDMS coated $NaLiFePO_4F$ electrode during the charging and discharging process. The value of D_{Li^+} can be calculated according to the following Eq. (3) [33]:

$$D_{Li^+} = \frac{4L^2}{\pi\tau}\left(\frac{\Delta E_s}{\Delta E_\tau}\right)^2 \quad (3)$$

where L (cm) and τ(s) are the electrode thickness and the time of the current pulse, and ΔE_s and ΔE_τ are the voltage change during the rest and current pulse. During the charging state, the diffusion coefficients of $NaLiFePO_4F$ control and coated electrodes are about 7.17×10^{-10} and 1.20×10^{-9} $cm^2·s^{-1}$, respectively (Figs. S8(a) and S8(c) in the ESM). During the discharging state, they are about 5.29×10^{-10} cm^2 s^{-1} and 1.89×10^{-9} $cm^2·s^{-1}$, respectively. The higher diffusion coefficient, the smaller over-potential and voltage drop of the PEDOT-PDMS coated $NaLiFePO_4F$ electrode (Figs. S8(b) and S8(d) in the ESM), demonstrating that the PEDOT-PDMS coating layer can improve the conductivity of the $NaLiFePO_4F$ electrode.

Figures 3(a) and 3(b) exhibit the voltage profiles of the

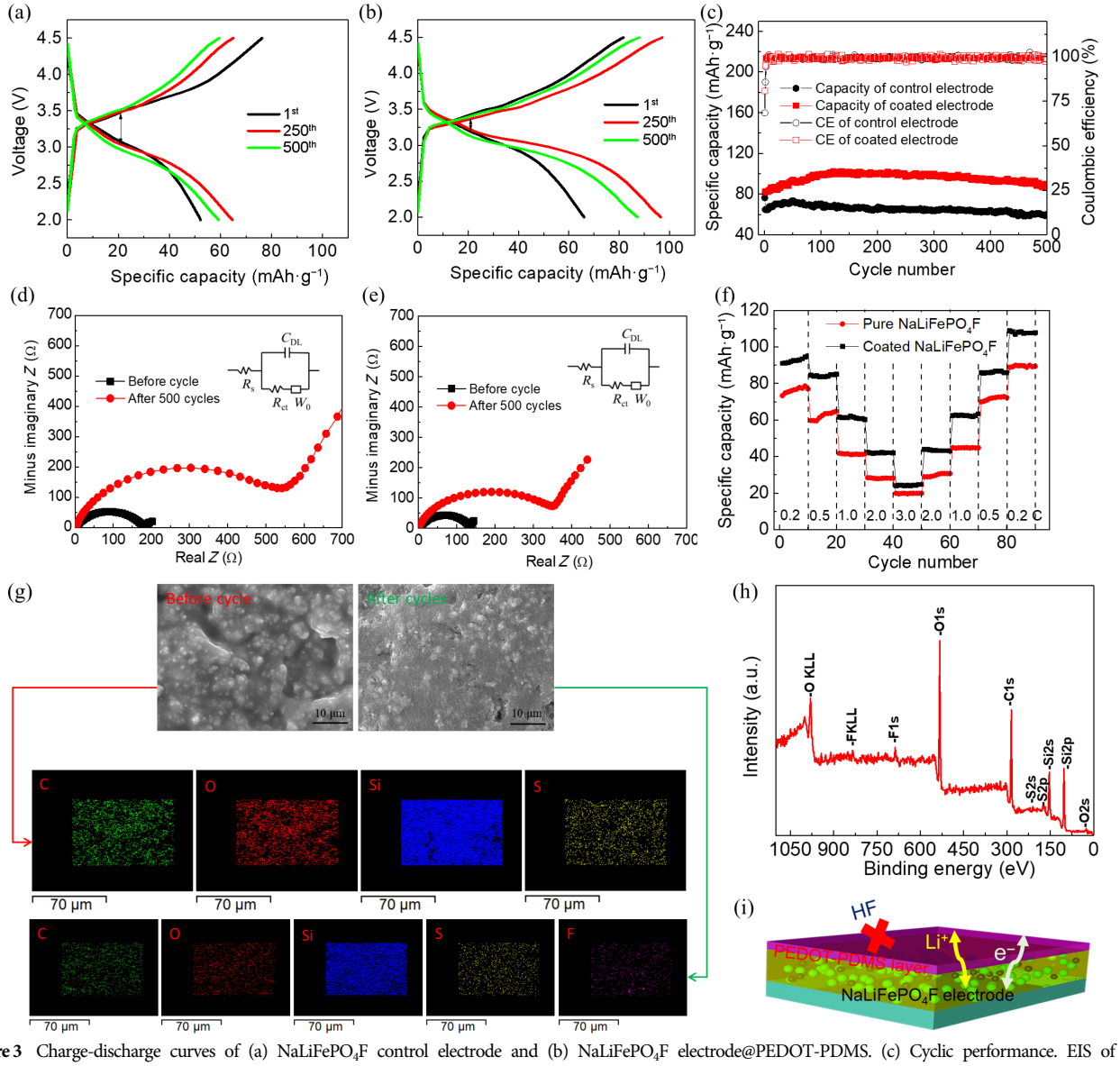

Figure 3 Charge-discharge curves of (a) $NaLiFePO_4F$ control electrode and (b) $NaLiFePO_4F$ electrode@PEDOT-PDMS. (c) Cyclic performance. EIS of (d) $NaLiFePO_4F$ control electrode and (e) $NaLiFePO_4F$ electrode@PEDOT-PDMS along with equivalent circuit. (f) Rate performance. (g) SEM images of $NaLiFePO_4F$ electrode@PEDOT-PDMS cathode before cycling and after cycling with the elemental distribution mapping. (h) XPS spectra of $NaLiFePO_4F$ electrode@PEDOT-PDMS electrode after cycling. (i) Schematic illustration of the effect of PEDOT-PDMS.

$NaLiFePO_4F$ control and PEDOT-PDMS coated $NaLiFePO_4F$ electrode, respectively. The initial charge and discharge capacity of the control electrode is 76.3 and 52.2 $mAh·g^{-1}$, respectively. The initial Coulombic efficiency is 68.4%. For the coated electrode, the initial charge and discharge capacity is 81.7 and 66 $mAh·g^{-1}$, and the corresponding initial Coulombic efficiency is 80.8%. After 500 cycles, the charge and discharge capacity of control electrode decrease to 59.5 and 59.2 $mAh·g^{-1}$, respectively, while the charge and discharge capacity of coated electrode increase to 88.1 and 87.3 $mAh·g^{-1}$, respectively. Compared with the $NaLiFePO_4F$ control electrode, the coated electrode shows a smaller polarization gap with cycling. The larger polarization of the $NaLiFePO_4F$ control electrode results from the limited Li-ion diffusion and charge transfer at the interface between electrolyte and electrode. The coated electrode shows better interfacial chemistry. The layer could enhance electron conductivity due to more PF_6^- doping with cycling. The polarization is responsible for the cyclability of batteries, which can lead to fast capacity decay of batteries. One can also note that the control electrode shows low voltage in the initial cycle than that after the 250th and 500th cycles, while the voltage of the coated ones show a reverse trend with cycling. For $NaLiFePO_4F$ control electrode during charging, the inner resistance of the battery cannot be avoided. However, the conducting capability of the coated electrode could be enhanced with cycling, which is confirmed by anodic peak shifting in CV curves. For the control electrode, the anodic peak shifts to a higher voltage with cycling, while it shifts to a lower voltage range with cycling for the coated electrode.

The cycling performance of $NaLiFePO_4F$ control and PEDOT-PDMS coated $NaLiFePO_4F$ electrodes is compared after up to 500 cycles at 0.5 C, as shown in Fig. 3(c). Their capacities show an increasing trend with cycling in the initial cycles. Such trend for the control electrode is completed after 50 cycles, while it lasts until about the 130th cycle for PEDOT-PDMS coated $NaLiFePO_4F$ electrode, which is due to slow Na^+ and Li^+ exchange, and the gradual penetration of electrolyte into the coating. The penetration of electrolyte can provide a sufficient amount of anions such as PF_6^- for doping, and the full use of active material. Thus, the

specific capacity of the coated electrode is higher than that of the control electrode all the time. The initial charge capacities of $NaLiFePO_4F$ control and PEDOT-PDMS coated $NaLiFePO_4F$ electrodes are 76.3 and 81.7 mAh·g^{-1}, respectively. The capacities are 59.5 and 88.1 mAh·g^{-1} after 500 cycles, showing 78%, 100% retention, respectively. The results indicate that PEDOT-PDMS polymer layer can improve the electrochemical stability of $NaLiFePO_4F$ electrodes, which has a close relationship with the enhancement of electron transfer at the interface between the electrode and electrolyte [32]. Besides, the polymer layer plays an important role in preventing HF production and protecting $NaLiFePO_4F$ from HF attack during cycles, resulting in no loss of active material. It should also be noted that the initial Coulombic efficiency for the coated electrode is 80.8% because of the consumption of a certain amount of the lithium in SEI and the insertion of Li^+ into the polymer in the first charge and discharge process. However, the value (80.8%) is much higher than that of the control electrode (68.4%) due to the coating protection leading to fewer side reactions.

To further evaluate the effect of PEDOT-PDMS on the electrochemical performance of $NaLiFePO_4F$, the EIS analysis of $NaLiFePO_4F$ control and coated electrodes are conducted before and after 500 cycles, and the results are shown in Figs. 3(d) and 3(e). These two electrodes exhibit a high-frequency semicircle corresponding to the charge transfer resistance (R_{ct}) and a low-frequency straight line associated with lithium-ion diffusion. The resistance is related to the activation polarization that occurs in the electrode-electrolyte charge transfer. The coated $NaLiFePO_4F$ electrode has smaller R_{ct} for the pristine electrode and that after 500 cycles (i.e., 140 and 380 Ω, respectively) than those of the control electrode (180 Ω and 590 Ω). The small increase in R_{ct} for the coated $NaLiFePO_4F$ electrode indicates the significant improvement in the interfacial kinetics because of the improved conductivity, resulting in a smaller polarization gap and better rate property, as shown in Fig. 3(f). The capacity of batteries fabricated with coated electrodes remains relatively high with rates varying from 0.2 C to 3.0 C and then returning to 0.2 C. With the increases of the current density, i.e., 0.5 C, 1.0 C, 2.0 C and 3.0 C, the coated electrode achieves capacities of 84.9, 60.2, 42.3, and 24.7 mAh·g^{-1}, respectively. When the battery is discharged back to lower current densities again, i.e., 2.0 C, 1.0 C, 0.5 C and 0.2 C, satisfactory reversible capacities are obtained, indicating good stability at different current densities. The better rate performance of the coated electrodes suggests the assistance of PEDOT-PDMS in suppressing the loss of active material and improving electrical and ionic conductivity, which has been confirmed by the GITT tests. Although the control electrode also delivers good stability at different current densities, the capacities are always relatively low. The capacity values of 64.3, 41.3, 28.7 and 19.6 mAh·g^{-1} are obtained at the rates of 0.5 C, 1.0 C, 2.0 C, and 3.0 C.

The SEM images of the coated electrode before (left) and after cycling of 500 times (right) are shown in Fig. 3(g). The PEDOT-PDMS layer shows excellent structural integrity and stability even after 500 cycles. It is because the conductive layer is stable without dissolution in the electrolyte. The surface of the PEDOT-PDMS layer becomes rough after cycling. Simultaneously, the surface elemental distribution of the coated electrode before and after cycling is evaluated by EDS mapping. In the case of the sample before cycling, the elements C, O, Si and S are distributed uniformly. Moreover, the presence of the elements in the EDS maps reveals that the PEDOT-PDMS layer is successfully formed on the surface of the $NaLiFePO_4F$ electrode. As for the sample after cycling, elements C, O, Si and S also appear and the distribution is still uniform, further indicating that the PEDOT-PDMS layer remains well on the $NaLiFePO_4F$ electrode surface after cycling. In addition, the element F is detected and no other elements such as P, Na, and Fe emerge, demonstrating that the F is derived from LiF of SEI composition instead of $LiPF_6$ electrolyte salt or $NaLiFePO_4F$ electrode. Moreover, it is known that the Na^+ ions can be replaced by Li^+ after cycling. However, there is no trace of Na in the polymer layer. The absence of Na in the maps of the coated electrode after cycling suggests the effective ion conductive performance of PEDOT-PDMS coating as Na^+ transfers through the polymer coating into the electrolyte. This observation is also supported by the XPS characterization of the coated electrode after cycling (Fig. 3(h)). The elements C, O, Si, S and F appear on the surface of the coated electrode after cycling. The PEDOT-PDMS can not only protect electrode from HF attack but also provide transportation path to ions and electrons (Fig. 3(i)). As a result, PEDOT-PDMS could be a potential protective coating material for the electrode used in energy storage devices to improve cycle stability.

Previous studies indicate that PEDOT-PDMS is expected to serve as a flexible and continuous three-dimensional structure, providing for volume buffer as well as ionic and electronic conduction. Hence, silicon nanoparticles (SiNP) are coated with PEDOT-PDMS polymer as a protective coating layer through *in-situ* synthesis to improve the cycling stability of Si (Fig. 4(a)). To confirm that PEDOT-PDMS has successfully formed into a layer on the surface of Si nanoparticles, TEM, FTIR, Raman, XPS and XRD measurements are performed for raw Si and coated Si nanoparticles. Compared with raw Si nanoparticles (Fig. S9 in the ESM), a foam-like network (indicated by arrows in blue) formed on the surface of Si after coating with PEDOT-PDMS (Fig. 4(b)), which cannot be detected in pure Si. The results indicate the presence of the coating layer on the surface of Si, and the intimate connection between the polymer matrix and Si nanoparticles. The thickness of the coating layer is 3–10 nm. The SAED patterns of pure Si nanoparticles (Fig. S10(a) in the ESM) show the Si (311), Si (220), and Si (111) crystallographic planes, indicating the dominant presence of crystalline Si phase[34]. However, the SAED patterns of the coated Si nanoparticles (Fig. S10(b) in the ESM) are diffusive, demonstrating the presence of a polymer layer coated on the surface of Si and that the coating material is amorphous [35].

In addition, the FTIR patterns of SiNP@PEDOT-PDMS are similar to those of PEDOT-PDMS polymer, while they are different from those of raw Si (Fig. 4(c)). Compared with the FTIR patterns of PEDOT-PDMS, there are no new peaks for the SiNP@PEDOT-PDMS sample. The interaction between PEDOT-PDMS and Si is based on the hydrogen bonding interaction, i.e., between Si-OH, owing to the presence of SiO_2 on the surface of Si particles and polymer molecules. One peak at 793 cm^{-1} is due to CH_3 rocking vibration and the Si-C stretching vibration. The peak around 1470 cm^{-1} is attributed to the new C=C band for PEDOT-PDMS [22]. The peaks at 1411 and 1260 cm^{-1} are ascribed to the deformation vibration and symmetrical vibrations of CH_3 groups; the peaks at 1085 and 1030 cm^{-1} are due to asymmetric and symmetric stretching of Si-O-Si, respectively [20]. Additionally, the characteristic peak at 2131 cm^{-1} for Si-H group in h_2PDMS disappears, illustrating the successful synthesis of PEDOT-PDMS on the surface of Si nanoparticles [21]. The peak around 695 cm^{-1} is related to in-plane deformation of C-S-C [36]. Furthermore, there is a new peak in Raman spectra for SiNP@PEDOT-PDMS

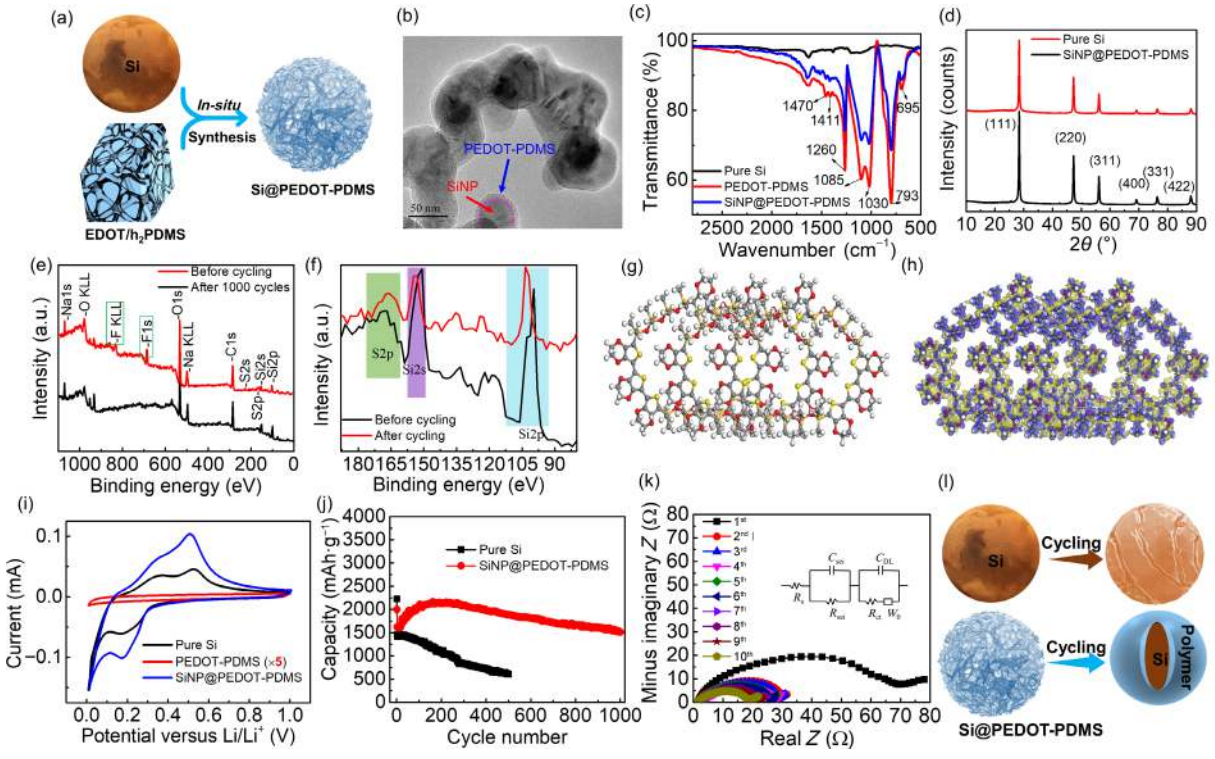

Figure 4 (a) Schematic illustration about synthesis of SiNP@PEDOT-PDMS. (b) TEM of SiNP@PEDOT-PDMS. (c) FTIR of pure Si, PEDOT-PDMS, and SiNP@PEDOT-PDMS. (d) XRD of pure Si and SiNP@PEDOT-PDMS. (e) XPS spectra and (f) S 2p, Si 2s, and Si 2p of SiNP@PEDOT-PDMS electrode before and after cycling. The electron distribution of PEDOT-PDMS (g) before and (h) during cycling. (i) CV curves of pure Si, PEDOT-PDMS electrode and SiNP@PEDOT-PDMS. (j) Cycle performance of Si control electrode and SiNP@PEDOT-PDMS electrode at 0.5 C. (k) The impedance tests of SiNP@PEDOT-PDMS electrode after each cycle between 1 and 10 along with equivalent circuit. (l) Schematic illustration about the change of pure Si and coated Si electrode after cycling.

and at the same time the other peaks shift to left (Fig. S11 in the ESM). Hence, all the results obtained from TEM, FTIR, and Raman demonstrate successful synthesis of PEDOT-PDMS on the surface of Si. The crystalline structure of raw Si nanoparticles and coated Si nanoparticles is characterized by using XRD (Fig. 4(d)). It can be observed from the patterns of plain Si that six obvious peaks located at 2θ of 28.4, 47.3, 56.1, 69.1, 76.3, and 88, which are indexed as the (111), (220), (311), (400), (331), and (422) crystal planes [37]. Moreover, no impurity peaks in the XRD patterns of SiNP@PEDOT-PDMS are detected, illustrating that PEDOT-PDMS has no effect on the crystalline structure of Si. The pure Si and coated Si electrodes exhibit different color (Fig. S12 in the ESM).

The XPS results show the elemental change of the SiNP@PEDOT-PDMS electrode before and after cycling, identifying the integrity of the PEDOT-PDMS coating. It can be seen that the new F peaks at 685.7 eV originate from HF adsorption (Fig. 4(e)). In addition, the peak of S 2p shifts to low binding energy (the green region in Fig. 4(f)) after cycling, indicating electron-donating groups (such as PF_6^-) appear around S. It is because π-π conjugated structure provides electrons transfer pathway and therefore the electron density increases. However, the peaks of Si 2s (purple area) and Si 2p (blue area) shift to high binding energy, implying the appearance of electronegative groups around Si. Hence, Li^+ transfers through Si-O in the amorphous phase. These results are also confirmed by density functional theory (DFT) calculation. Before cycling, the structure of PEDOT-PDMS is shown in Fig. 4(g). There is no dopants and ions. However, electron enrichment area, i.e., the yellow area, appears around π-π conjugated structure during cycling (Fig. 4(h)). The calculated D_{Li^+} for Si control electrode is around 5.07×10^{-13} $cm^2\cdot s^{-1}$ (Fig. S13 in the ESM). However, for the coated Si electrode, it is over thirty times that of Si control electrode (2.47×10^{-11} $cm^2\cdot s^{-1}$). In addition, the voltage drop caused by the internal resistance for the coated electrode is smaller than that of Si control one, which benefits the electrochemical performance of the batteries. The obtained results further illustrate the PEDOT-PDMS coating has the capability of improving the lithium-ion conductivity of the Si electrode, reducing the resistance and polarization effect.

To study the electrochemical performances of SiNP@PEDOT-PDMS, CV measurement is carried out (0.1 $mV\cdot s^{-1}$) (Fig. 4(i)). The CV plot for SiNP@PEDOT-PDMS electrode shows typical electrochemical behavior, i.e., there are typical lithiation and delithiation peaks, which are similar to that of graphene caged silicon nanoparticles electrode. The SiNP@PEDOT-PDMS electrode shows a larger area of the current vs. voltage curve than that of SiNP electrode, implying a larger specific capacity of SiNP@PEDOT-PDMS electrode. Moreover, to evaluate the contribution of PEDOT-PDMS to the specific capacity of the whole batteries, the CV and electrochemical cycling performance of pure PEDOT-PDMS electrode without binder and super P is measured on half cells. The CV curve for PEDOT-PDMS electrode shows a much lower current than that for SiNP@PEDOT-PDMS, even if it is magnified five times. Moreover, the current is very stable and does not show any fluctuation. The results indicate that the contribution of PEDOT-PDMS to the capacity of the whole electrode is negligible, which also can be further supported by the cycle performance of PEDOT-PDMS electrode (Fig. S14 in the ESM). The specific capacitance is between 1 and 2 $mAh\cdot g^{-1}$, therefore it is negligible compared with that of silicon. In addition, it can also be seen that the capacity is very stable even after 1000 cycles, indicating good electrochemical stability of PEDOT-PDMS polymer during cycling.

As for the cycling performance (Fig. 4(j)), the Si coated

electrode shows an increase in the capacity during the initial cycles, while this behavior cannot be observed for the raw Si control electrode, which is due to the delayed wetting of electrolyte into the coated Si electrode. It also can be seen that the Si control electrode delivers a dramatic decay in specific capacity at 0.5 C, losing over 70% of its first specific capacitance after 500 cycles (~605 mAh·g^{-1}). In comparison, the coated Si electrode shows good cyclic stability at 0.5 C. A specific capacitance of ~1512 mAh·g^{-1} is still there after cycling of 1000 times, corresponding to ~69.8% capacity retention according to the highest specific capacity around the 160th cycle (~2166 mAh·g^{-1}). The obtained results are better than or comparable to the results of previously reported Si particle-based anode works as listed in Table S1 in the ESM. The results can be ascribed to the PEDOT-PDMS polymer skin that could buffer the huge volume change of Si anode, leading to the formation of a more stable SEI in cycling. The Coulombic efficiency can indicate the stability of the SEI due to Li consumption during SEI rupturing and reforming. For SiNP@PEDOT-PDMS electrode, the corresponding initial Coulombic efficiency is 77.44%, which is higher than that of Si control electrode (~67.74%) (Figs. S15 and S16 in the ESM), owing to few side reactions. The Coulombic efficiency of the coated electrode from the 3rd cycle increases to 99.24%, which is faster than that of the Si control electrode (increase to 98.57% after 6 cycles), indicating the quick formation of the stable SEI outside the coated electrode. However, for the coated electrode, the initial Coulombic efficiency is still low due to the stable SEI built on the outside of the PEDOT-PDMS layer and the insertion of Li^+ into PEDOT-PDMS, consuming a certain amount of lithium. The continuously conductive PEDOT-PDMS matrix also provides conducting pathways for fast electron and Li^+ transference which has been evaluated by GITT and will be further evaluated by using EIS.

The Nyquist curves for Si control anode and SiNP@PEDOT-PDMS anode after different cycles include a semicircle at high-frequency and a low-frequency straight line (Fig. 4(k) and Fig. S17 in the ESM). The high-frequency semicircle is associated to the combined resistance of SEI layer (R_{sei}) and charge transfer resistance (R_{ct}), as well as the contact interface resistance (R_{int}). The straight line at low-frequency is associated to the Warburg impedance (Z_w), i.e., lithium diffusion in the electrode materials. In the case of Si control anode, the semicircles undergo a reduction process in the first seven cycles but show obvious changes for the later cycles, reaching ~60 Ω at the 10th cycle. However, in the case of the coated electrode, the semicircle shrinks for the first few cycles, and no obvious increase in semicircle can be observed afterwards, keeping at around 20 Ω, which is much lower than that of Si control electrode. In addition, the semicircle for Si control anode is larger than that for the coated anode after the first cycle. The phenomenon may be due to the following reasons: Firstly, after the first cycle, both of the cells fabricated with Si control anode and SiNP@PEDOT-PDMS anode have high R_{int} and R_{ct}; however, for the bare anode, R_{sei} is larger due to naked Si. Secondly, as for the coated anode, the conductivity increases after Li^+ and PF_6^- doping and the SEI film is stable due to the capability of accommodating volume expansion, leading to smaller and more stable semicircles; for the Si control anode, after several cycles, the SEI film starts to crack, resulting in the straightforward contact between Si and electrolyte again, and the formation of more SEI films and high R_{sei}. Hence, the semicircle radius increases after seven cycles and the Coulombic efficiency of Si control electrode is lower than that of SiNP@PEDOT-PDMS electrode in the initial several cycles. In the rate performance test, the cells are firstly activated for five cycles at 0.05 C and then tested at 0.2 C, 0.5 C, 0.8 C, and 1.0 C every twenty cycles (Fig. S18 in the ESM). The capacitance of a SiNP@PEDOT-PDMS electrode varies from ~2411 mAh·g^{-1} to ~1166 mAh·g^{-1} at charging and discharging rate varying from 0.2 C to 1.0 C, which is over twice larger than that of conventional graphite electrode (1 C, 372 mAh·g^{-1}).

The difference between Si control electrode and SiNP@PEDOT-PDMS electrode after cycling is illustrated in Fig. 4(l). Some undesirable cracks appear on the surface and inside the Si control electrode, while the SiNP@PEDOT-PDMS electrode still remains integrated without cracks on the surface and the interiors, which highlight the coated electrode suffered from smaller volume change during charge-discharge. The results can be verified in the surface and the cross-sectional SEM images (Fig. S19 in the ESM). Obviously, the cross-sectional images that the unlimited growth of SEI appears in the control electrode. In comparison, the stable SEI forms in the coated electrode. The obtained results directly indicate that the PEDOT-PDMS coating plays a positive role in suppressing volume change and limiting SEI growth of Si electrode during charging and discharging processes.

The *in-situ* TEM is used to further directly confirm how the PEDOT-PDMS coating affects the electrochemical lithiation of Si particles. Figures 5(a)–5(c) captured from Movie 1 in the ESM show the initial lithiation process of the pure Si particle with ~95.81 nm in diameter before lithiation. Through comparing the volume change of the Si or coated Si nanoparticles (yellow arrows) that are near the Li source, it can be found that, after lithiation (Fig. 5(b)) for pure Si, an amorphous shell is formed on the surface of crystalline Si core because of the lithiation; After further lithiation to 210 s, the diameter of Si particle grows to ~122.16 nm (Fig. 5(c)) while the crystalline Si core still can be observed, indicating the incomplete lithiation because of the retardation effect of the stress induced by the lithiation. In addition, the pure Si particles that are far away (~288.41 nm) from the lithium (red arrows and red circles in Figs. 5(b) and 5(c)) do not show the lithiation process even after lithiation for 100 s because of the retardation effect. However, the lithiation could occur for the coated Si particles that are far away (~329.10 nm) from the lithium only after lithiation for 50 s (red arrows and red circles in Figs. 5(e) and 5(f)) since the coating could buffer the stress and provide conducting pathways, in consistent with the GITT, EIS results. On the other hand, the diameter of coated Si particle shows a bigger change from ~98.51 to ~129.10 nm (Figs. 5(d)–5(f)), indicating that there are more amount of Li lithiated inside the coated Si and smaller self-limiting lithiation since the coat could buffer the stress during the cycling processes, which are consistent with the SEM results. Hence, the *in-situ* TEM results further confirm the enhanced electrochemical performance of the coated electrode.

4 Summary

To effectively optimize high-voltage $NaLiFePO_4F$ cathode and high-capacity Si anode, the desired electron/ionic-conductive and flexible copolymer PEDOT-PDMS is successfully synthesized from h_2PDMS and EDOT. Theoretical calculation and experiments indicate that π-π conjugated structure in PEDOT-PDMS molecular chains provide electron transfer pathways and prevent HF production, and Li ions transfer through Si-O segments. Its Young's modulus at rupture is 1.17±0.10 MPa. $NaLiFePO_4F$ electrode@PEDOT-PDMS shows high specific

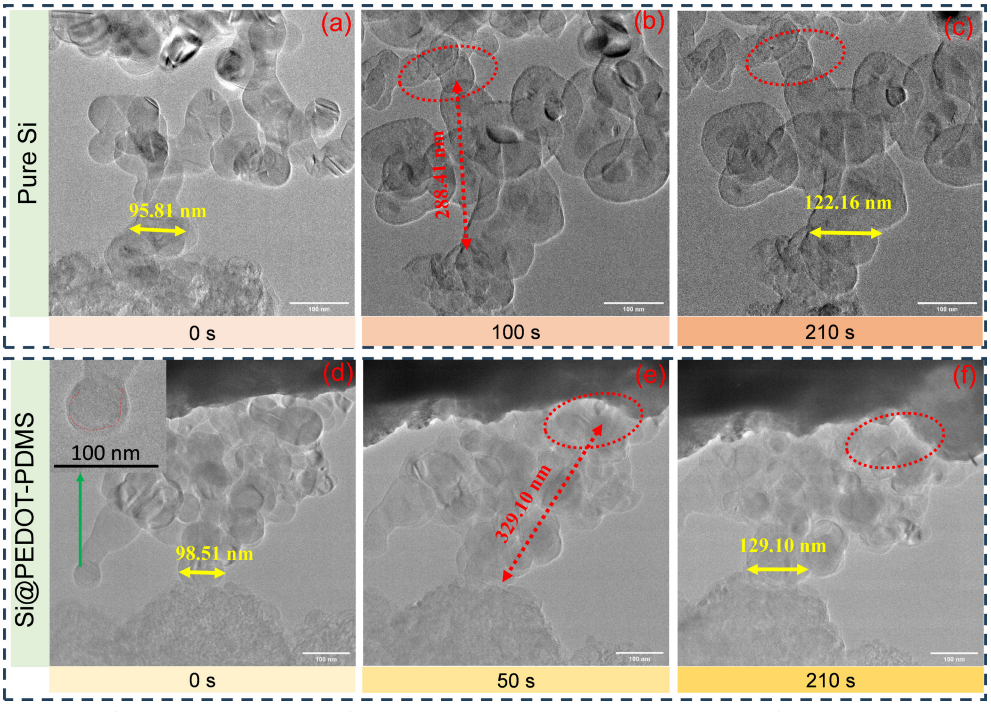

Figure 5 TEM images captured from Movie 1 in the ESM of pure Si particle (a)-(c) and Movie 2 in the ESM of SiNP@PEDOT-PDMS particle (d)-(f) during lithiation, two movies are played at 7 times of the real speed.

capacity, good cycle stability and high D_{Li^+} compared to $NaLiFePO_4F$ control electrode. The *in-situ* TEM results directly confirm that it provides conducting pathways and buffers the stress induced by lithiation. The lithiation could occur for SiNP@PEDOT-PDMS that are far away from the Li_2O/Li electrode, while raw Si particles do not show the lithiation process. The D_{Li^+} for SiNP@PEDOT-PDMS electrode is over thirty times that of Si control one. The copolymer PEDOT-PDMS could be also a potential material for optimizing other electrode materials.

Acknowledgements

The authors are grateful for the following financial supports: National Natural Science Foundation of China (Grant Nos. 22109103, 52205489, 52372289 and 52102368), Guangdong Science and Technology Bureau (Grant Nos. 2019B090908001 and 2020A0505090011), Shenzhen STI (Grant No. SGDX20190816230615451), Guangdong-Hong Kong-Macao Joint Laboratory for Photonic-Thermal-Electrical Energy Materials and Devices (Grant No. 2019B121205001), Otto Poon Charitable Foundation (Grant Nos. 847W, CDBC, CDBW).

Declaration of conflicting interests

The authors declare no conflicting interests regarding the content of this article.

Data availability

All data needed to support the conclusions in the paper are presented in the manuscript and/or the Supplementary Materials. Additional data related to this paper may be requested from the corresponding author upon request.

Electronic Supplementary Material: Supplementary material (materials and preparation, cell assembly, electrochemical testing conditions of $NaLiFePO_4F$@PEDOT-PDMS and SiNP@PEDOT-PDMS, theory calculation, PEDOT-PDMS characterizations and electrochemical test (NMR spectra, cycle performance, CV), $NaLiFePO_4F$ electrode and $NaLiFePO_4F$@PEDOT-PDMS electrode characterizations and electrochemical test (EDS, EIS, cycle performance, GITT), pure Si nanoparticle and SiNP@PEDOT-PDMS characterizations and electrochemical test (TEM, Raman, SEM, GITT, cycle performance, EIS, charge-discharge curves, voltage profiles), comparison of our work with published reports) is available in the online version of this article at https://doi.org/10.26599/NRE.2022.9120133.

References

[1] Xu, J. J.; Zhang, J. X.; Pollard, T. P.; Li, Q. D.; Tan, S.; Hou, S.; Wan, H. L.; Chen, F.; He, H. X.; Hu, E. Y. et al. Electrolyte design for Li-ion batteries under extreme operating conditions. *Nature* **2023**, *614*, 694–700.

[2] Li, Z. W.; Han, M. S.; Yu, P. L.; Lin, J. S.; Yu, J. Macroporous directed and interconnected carbon architectures endow amorphous silicon nanodots as low-strain and fast-charging anode for lithium-ion batteries. *Nano-Micro Lett.* **2024**, *16*, 98.

[3] Su, C.; Gao, X.; Liu, K. J.; Dai, Y. H.; Dong, H. B.; Liu, Y. Y.; Zhu, J. Y.; Zhang, Q. X.; He, H. Z.; He, G. J. From lab to market: A review of commercialization and advances for binders in lithium-, zinc-, sodium-ion batteries. *Nano Res. Energy* **2024**, *3*, e9120094.

[4] Xu, G. L.; Liu, J. Z.; Amine, R.; Chen, Z. H.; Amine, K. Selenium and selenium-sulfur chemistry for rechargeable lithium batteries: Interplay of cathode structures, electrolytes, and interfaces. *ACS Energy Lett.* **2017**, *2*, 605–614.

[5] Wu, Y.; Ma, F.; Zhang, Z. H.; Chen, D. Q.; Yu, H. S.; Zhang, X. J.; Ding, F.; Zhang, L.; Chen, Y. F. Amorphous lithiophilic cobalt-boride@rGO interlayer for dendrite-free and highly stable lithium metal batteries. *EcoEnergy* **2024**, *2*, 299–310.

[6] Wu, H.; Cui, Y. Designing nanostructured Si anodes for high energy lithium ion batteries. *Nano Today* **2012**, *7*, 414–429.

[7] Shen, J.; Zhang, S. L.; Wang, H. L.; Wang, R. X.; Hu, Y. Y.; Mao, Y. Y.; Wang, R. L.; Zhang, H. H.; Du, Y. M.; Fan, Y. M. et al. Unlocking the potential of silicon anodes in lithium-ion batteries: A

claw-inspired binder with synergistic interface bonding. *eScience* **2024**, *4*, 100207.
[8] Hu, W. F.; Li, Y. Y.; Liu, J. P. Pressure-induced pre-lithiation enables high-performing Si anodes in all-solid-state batteries. *Energy Environ. Mater.*, in press, DOI: 10.1002/eem2.12786.
[9] Du, F. H.; Wang, K. X.; Chen, J. S. Strategies to succeed in improving the lithium-ion storage properties of silicon nanomaterials. *J. Mater. Chem. A* **2016**, *4*, 32–50.
[10] Wang, J. W.; Zhao, Z. J.; Hu, F.; Song, H. Q.; Xie, Q. R.; Wan, X. J.; Song, S. H. Highly reversible Zn metal anodes enabled by multifunctional poly zinc acrylate protective coating. *Chem. Eng. J.* **2023**, *451*, 139058.
[11] Li, L.; Nam, J.S.; Kim, M. S.; Wang, Y. F.; Jiang, S. H.; Hou, H. Q.; Kim, I. D. Sulfur-carbon electrode with PEO-LiFSI-PVDF composite coating for high-rate and long-life lithium-sulfur batteries. *Adv. Energy Mater.* **2023**, *13*, 2302139.
[12] Xiao, B. W.; Sun, X. L. Surface and subsurface reactions of lithium transition metal oxide cathode materials: An overview of the fundamental origins and remedying approaches. *Adv. Energy Mater.* **2018**, *8*, 1802057.
[13] Zeng, G. F.; Sun, Q.; Horta, S.; Wang, S.; Lu, X.; Zhang, C. Y.; Li, J.; Li, J. S.; Ci, L. J.; Tian, Y. H.; Ibáñez, M.; Cabot, A. A layered Bi_2Te_3@PPy cathode for aqueous zinc-ion batteries: Mechanism and application in printed flexible batteries. *Adv. Mater.* **2023**, *36*, 2305128.
[14] Zhang, F.; Xiong, P.; Guo, X.; Zhang, J. Q.; Yang, W.; Wu, W. J.; Liu, H.; Wang, G. X. A nitrogen, sulphur dual-doped hierarchical porous carbon with interconnected conductive polyaniline coating for high-performance sodium-selenium batteries. *Energy Storage Mater.* **2019**, *19*, 251–260.
[15] Xu, G. L.; Liu, Q.; Lau, K. K. S.; Liu, Y. Z.; Liu, X.; Gao, H.; Zhou, X. W.; Zhuang, M. H.; Ren, Y.; Li, J. D. et al. Building ultraconformal protective layers on both secondary and primary particles of layered lithium transition metal oxide cathodes. *Nat. Energy* **2019**, *4*, 484–494.
[16] Raza, H.; Bai, S. Y.; Cheng, J. Y.; Majumder, S.; Zhu, H.; Liu, Q.; Zheng, G. P.; Li, X. F.; Chen, G. H. Li–S batteries: Challenges, achievements and opportunities. *Electrochem. Energy Rev.* **2023**, *6*, 29.
[17] Wang, M. J.; Wang, W. K.; Wang, A. B.; Yuan, K. G.; Miao, L. X.; Zhang, X. L.; Huang, Y. Q.; Yu, Z. B.; Qiu, J. Y. A multi-core-shell structured composite cathode material with a conductive polymer network for Li–S batteries. *Chem. Commun.* **2013**, *49*, 10263–10265.
[18] Zhu, B.; Jin, Y.; Hu, X. Z.; Zheng, Q. H.; Zhang, S.; Wang, Q. J.; Zhu, J. Poly(dimethylsiloxane) thin film as a stable interfacial layer for high-performance lithium-metal battery anodes. *Adv. Mater.* **2017**, *29*, 1603755.
[19] Meng, J. W.; Chu, F. L.; Hu, J. L.; Li, C. L. Liquid polydimethylsiloxane grafting to enable dendrite-free Li plating for highly reversible Li-metal batteries. *Adv. Funct. Mater.* **2019**, *29*, 1902220.
[20] Zengin, A.; Badak, M. U.; Bilici, M.; Suludere, Z.; Aktas, N. Preparation of molecularly imprinted PDMS elastomer for selective detection of folic acid in orange juice. *Appl. Surf. Sci.* **2019**, *471*, 168–175.
[21] Klasner, S. A.; Metto, E. C.; Roman, G. T.; Culbertson, C. T. Synthesis and characterization of a poly(dimethylsiloxane)-poly(ethylene oxide) block copolymer for fabrication of amphiphilic surfaces on microfluidic devices. *Langmuir* **2009**, *25*, 10390–10396.
[22] Chen, R.; Sun, K.; Zhang, Q.; Zhou, Y. L.; Li, M.; Sun, Y. Y.; Wu, Z.; Wu, Y. Y.; Li, X. L.; Xi, J. L. et al. Sequential solution polymerization of poly(3,4-ethylenedioxythiophene) using V_2O_5 as oxidant for flexible touch sensors. *iScience* **2019**, *12*, 66–75.
[23] Wei, B.; Liu, J. L.; Ouyang, L. Q.; Martin, D. C. POSS-ProDOT crosslinking of PEDOT. *J. Mater. Chem. B* **2017**, *5*, 5019–5026.
[24] Risangud, N.; Li, Z. J.; Anastasaki, A.; Wilson, P.; Kempe, K.; Haddleton, D. M. Hydrosilylation as an efficient tool for polymer synthesis and modification with methacrylates. *RSC Adv.* **2015**, *5*, 5879–5885.
[25] Sharma, P.; Patel, D. K.; Kancharlapalli, S.; Magdassi, S.; Sasson, Y. Facile combined experimental and computational study: g-C_3N_4@PDMS-assisted Knoevenagel condensation reaction under phase transfer conditions. *ACS Sustain. Chem. Eng.* **2020**, *8*, 2350–2360.
[26] Lee, S.; Gleason, K. K. Enhanced optical property with tunable band gap of cross-linked PEDOT copolymers via oxidative chemical vapor deposition. *Adv. Funct. Mater.* **2015**, *25*, 85–93.
[27] Kayser, L. V.; Russell, M. D.; Rodriquez, D.; Abuhamdieh, S. N.; Dhong, C.; Khan, S.; Stein, A. N.; Ramírez, J.; Lipomi, D. J. RAFT polymerization of an intrinsically stretchable water-soluble block copolymer scaffold for PEDOT. *Chem. Mater.* **2018**, *30*, 4459–4468.
[28] Noh, J. S. Highly conductive and stretchable poly(dimethylsiloxane): Poly(3,4-ethylenedioxythiophene):Poly(styrene sulfonic acid) blends for organic interconnects. *RSC Adv.* **2014**, *4*, 1857–1863.
[29] Klonos, P.; Sulym, I. Y.; Borysenko, M. V.; Gun'ko, V. M.; Kripotou, S.; Kyritsis, A.; Pissis, P. Interfacial interactions and complex segmental dynamics in systems based on silica-polydimethylsiloxane core-shell nanoparticles: Dielectric and thermal study. *Polymer* **2015**, *58*, 9–21.
[30] Kayser, L. V.; Lipomi, D. J. Stretchable conductive polymers and composites based on PEDOT and PEDOT:PSS. *Adv. Mater.* **2019**, *31*, 1806133.
[31] Lin, Z. Y.; Guo, X. W.; Yu, H. J. Amorphous modified silyl-terminated 3D polymer electrolyte for high-performance lithium metal battery. *Nano Energy* **2017**, *41*, 646–653.
[32] Ahn, J.; Yoon, S.; Jung, S. G.; Yim, J. H, Cho, K. Y. A conductive thin layer on prepared positive electrodes by vapour reaction printing for high-performance lithium-ion batteries. *J. Mater. Chem. A* **2017**, *5*, 21214–21222.
[33] Chang, Q.; Fu, X. L.; Gao, J. C.; Zhang, Z. H.; Liu, X.; Huang, C. S.; Li, Y. L. Advanced multilayered electrode with planar building blocks structure for high-performance lithium-ion storage. *Adv. Mater.* **2023**, *35*, 2305317.
[34] Cai, R.; Wang, Y.; Wang, J. R.; Zhang, J. F.; Yu, C. P.; Qin, Y. Q.; Cui, J. W.; Zhang, Y.; Tiwary, C. S.; Wu, Y. C. Accelerated hydrogen production on atomically thin silicon nanosheets photocatalyst with unique surface adsorption chemistry. *Int. J. Hyd. Energy* **2024**, *51*, 929–935.
[35] Eslamisaray, M. A.; Wray, P. R.; Lee, Y.; Nelson, G. M.; Ilic, O.; Atwater, H. A.; Kortshagen, U. R. A single-step bottom-up approach for synthesis of highly uniform mie-resonant crystalline semiconductor particles at visible wavelengths. *Nano Lett.* **2023**, *23*, 1930–1937.
[36] Kvarnström, C.; Neugebauer, H.; Blomquist, S.; Ahonen, H. J.; Kankare, J.; Ivaska, A. *In situ* spectroelectrochemical characterization of poly(3,4-ethylenedioxythiophene). *Electrochim. Acta* **1999**, *44*, 2739–2750.
[37] Wang, M. S.; Wang, G. L.; Wang, S.; Zhang, J.; Wang, J.; Zhong, W.; Tang, F.; Yang, Z. L, Zheng, J. M.; Li, X. *In situ* catalytic growth 3D multi-layers graphene sheets coated nano-silicon anode for high performance lithium-ion batteries. *Chem. Eng. J.* **2019**, *356*, 895–903.

Jingwei Wang received her Dual PhD degree from Harbin Institute of Technology in 2020 and The Hong Kong Polytechnic University in 2021 under the co-supervision of Prof. Shenhua Song and Prof. Guohua Chen. She is currently a senior lecture at Shenzhen MSU-BIT University. She is focusing on the fabrication and modification of polymer and their applications in energy storage devices.

Junye Cheng received his Ph.D. degree from City University of Hong Kong in 2019. Currently, he is an Associate Professor at Shenzhen MSU-BIT University. His current research interests focus on the development of low-dimensional nanomaterials for applications in energy storage and conversion, environmental protection, as well as electromagnetic wave absorption.

Guohua Chen obtained his B.Eng. degree from Dalian University of Technology in 1984, M.Eng. and Ph.D. degrees from McGill University, respectively, in 1989 and 1994. Now he is Chair Professor at City University of Hong Kong. Professor Chen's research is in the area of developing advanced materials for lithium/sodium ion batteries and Li-S batteries. He is a Fellow of HKIE, AIChE, Global Academy of Chinese Chemical Engineers. He is also elected as a Fellow of the Canadian Academy of Engineering.